Angulo-spectral surface plasmon resonance imaging of nanofabricated grating surfaces

Mohamed Nakkach, Aurélien Duval, Buntha Ea-Kim, Julien Moreau, Michael Canva

Angulo-spectral surface plasmon resonance imaging of nanofabricated grating surfaces

Mohamed Nakkach,[1,2,*] Aurélien Duval,[1] Buntha Ea-Kim,[1] Julien Moreau,[1] and Michael Canva[1]

[1]*Laboratoire Charles Fabry de l'Institut d'Optique Institut d'Optique Graduate School, Univ. Paris-Sud, CNRS Campus Polytechnique, RD 128, 91127 Palaiseau cedex, France*

[2]*Laboratoire de Spectroscopie Atomique Moléculaire et Applications, Faculté des Sciences, Tunis 1060, Tunisia*

**Corresponding author: mohamed.nakkach@u-psud.fr*

Received April 14, 2010; accepted May 14, 2010;
posted June 11, 2010 (Doc. ID 127015); published June 23, 2010

We present a surface plasmon resonance imaging (SPRI) setup, based on the Kretschmann configuration, capable of simultaneously acquiring the complete spectral and angular plasmonic reflectivity response on all points of the sensing area. Several line poly(methyl methacrylate) grating regions were fabricated on a thin-film gold surface and characterized with this SPRI system. Reflectivity maps of the corrugated regions showing plasmon bandgaps were obtained to illustrate the capability of the setup.

OCIS codes: 240.6680, 220.4241.

A surface plasmon wave (SPW) is a boundary electromagnetic wave propagating at the interface between a metal and a dielectric, characterized by its plasmon wave vector K_{sp}. In the Kretschmann configuration, an incident TM polarized wave, coming from a high refractive index medium, falls onto the metallic layer. A sharp resonance is obtained when the incident light wave vector K_x and the plasmon wave vector K_{sp} are made equal. Surface plasmon resonance (SPR) is very sensitive to the variations of thickness and refractive index in the vicinity of the metal–dielectric interface. This phenomenon is used in realizing sensors able to detect optical parameter variations induced by molecular interactions in the vicinity of the surface, such as biofilm thickness with subnanometric resolution. Several setups based on angular interrogation at a fixed wavelength or spectral interrogation at a fixed incident angle have been developed [1]. Measuring the reflectivity difference between two perpendicular SPR imaging (SPRI) sensor arms allows the determination of the anisotropy of biomolecular thin films [2]. A spectroimaging sensor based on SPR spectra measured off a diffraction grating showed a tenfold sensitivity enhancement [3]. Another setup based on simultaneous angular and spectral interrogations can be used to determinate the refractive index of dielectrics [4]. However, to our knowledge, none of these spectro-angular setups have imaging capabilities, which is of prime importance in multiplex biodetection systems. The integration of absorbing molecules [5] or nanoparticles [6] to the target molecules enhances the SPR signal, but the experiment loses its label-free characteristics. Nanopatterning the sensitive surface is an alternative for enhancing the response and reducing the effective reacting area [7]. Nanopatterning a dielectric or the metallic layer, in the form of a line grating on the surface of the prism, modifies the coupling condition.

Dielectric or metallic line gratings on a prism base have been used to realize sensors using the surface plasmon bandgap induced by the corrugation of the surface [4,8–10]. However, detection schemes using a line grating prove to be critically dependent on the fabrication accuracy of the grating periods and duty cycle. For example, in the case of a single excitation wavelength, a small error in the period or the duty cycle of the grating induces a large difference from the theoretical optimum of detection, drastically reducing the sensitivity of the system. This is why an agile system, easily tunable in its angular and spectral dimensions, would be of upmost importance.

In this Letter, we present a SPRI setup based on both angular and spectral interrogations using the Kretschmann configuration. Its multiparametric interrogation capabilities enable the acquisition of two-dimensional (2D) reflectivity images of the sample surface under various incidence angles and wavelengths. Processing these images gives access to several nanopatterned regions of the sample simultaneously. These plasmonic reflectivity response maps are directly related to the dimensions of the nanopatterning, as well as to the dispersion laws of the material used. Furthermore, it allows one to find the optimum working point $(\theta_0, \lambda_o))$ for dynamic SPRI measurements, even in the presence of not perfectly controlled pattern parameters, such as grating period or duty cycle.

The SPRI setup presented here is depicted in Fig. 1. A monochromator illuminated with a white-light halogen lamp generates in its output a tunable light source in the 600–850 nm range with a FWHM of 6 nm, thus avoiding speckle patterns in the image. Light is collected with an optical fiber and sent into the illumination system, made of a collimator, a polarizer, a mirror, and an afocal system (consisting of two $f = 60$ mm achromatic lenses) in order to conjugate the motorized rotating mirror with the gold surface. This illumination system fixed on a mechanical arm can rotate around the fixed base containing the prism, so that the central excitation angle can be changed from 50° to 79°. Once the central angle of incidence has been fixed, a stepper motor on the mirror allows precise scanning of the angular dependency of the reflectivity with a total angular amplitude of 7.5° around the central angle and a resolution of 0.028°. The second afocal system (two $f = 60$ mm achromatic lenses) conjugates the gold surface with the CCD camera (PixelFly QE, 12 bits). The microfluidic part is formed by a cell of 150 μm in depth and 1 cm in diameter, and a peristaltic pump is used to inject the analyte in a continuous flow. The temperature of the cell is kept constant with a 0.01 °C resolution using a Peltier module controlled in real time with a homemade program using LabVIEW

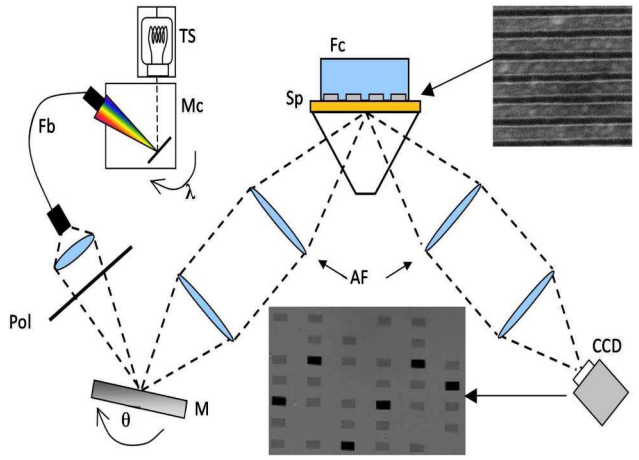

Fig. 1. (Color online) Experimental setup. TS, thermal light source; Mc, monochromator; Fb, optical fiber; Pol, polarizer; M, mirror; AF, afocal system; Sp, sample; Fc, fluidic cell; CCD, camera. Insets: top, SEM image of a grating area (image dimensions 2 μm × 1.7 μm); bottom, SPR image of the gold surface showing grating areas and reference areas (image dimensions 7 mm × 7 mm). The dark and the gray squares correspond, respectively, to the uniform gold (reference) and the grating areas.

(National instruments). Angular, spectral, or complete angulo-spectral reflectivity interrogation modes are possible, while maintaining imaging capabilities. For each incident angle and wavelength, we capture a TE image as a reference and then a TM image. The ratio between the TM and TE images gives us the corresponding reflectivity. Spatial resolution is limited by pixel sampling (approximately 7 μm). The imaging area is approximately 9 mm × 9 mm.

To illustrate the functionalities of our setup, we have fabricated several line grating regions, of 400 μm × 400 μm, on the same gold surface. These gratings consist of poly (methyl methacrylate) (PMMA) ridges surrounded by water, deposited on a uniform 55 nm gold layer and a 2 nm chromium adhesion layer. All gratings were realized using the same process to enable direct comparison among the different regions. Chromium and gold were evaporated on a SF10 glass slide. A PMMA resist (molecular weight 950k in 4% anisol) was then spin coated (4000 rpm during 20 s) on the gold surface in order to obtain a uniform ≈300 nm thick resist. Electron beam lithography (a dose of 7 C/m^2) was then used to imprint gratings on the bulk of the PMMA. Finally, the resist was developed in a methyl isobutyl ketone and isopropanol solution (1:3) for 40 s. The resulting gratings, characterized by using scanning electron microscopy (SEM), are depicted in the top inset of Fig. 1. The grating period was measured to be 250 nm, and the duty cycle of the PMMA ridges was approximately 30%. The grating period and duty cycle were calculated using rigorous coupled-wave analysis (RCWA) techniques (data not shown) in order to obtain a surface plasmon bandgap in the visible region.

These grating surfaces were experimentally characterized using our multiparametric SPRI system. The sample was deposited on the base of an equilateral SF10 glass prism using index matching oil (Cargille Laboratories Inc.). The microfluidic cell was then filled with purified water. Images of the surface were taken for incidence angles ranging from 56.78° to 63.35° (incident angle on gold from the normal) in steps of 0.33° and for wavelengths ranging from 600 to 850 nm in steps of 5 nm. Each reflectivity image was obtained by dividing the TM-polarized image by its corresponding TE-polarized image. An example of such an image of the sample surface is shown in Fig. 1 (bottom inset). Once this stack of images is acquired, the spectro-angular plasmonic reflectivity response $R_n(\theta, \lambda)$ on any point n of the sample surface can be extracted. They are normalized by a previously acquired plasmonic reflectivity response of the bare glass prism covered only with the water-filled microfluidic cell in order to compensate the spectral dependencies of the optical elements of the system. Figure 2 shows the reflectivity maps extracted from the normalized SPR data, using a spatial averaging of ≈300 μm × 300 μm on the grating regions. Figure 2(a) is taken from an area where no grating was fabricated, yielding a spectro-angular SPR dip typical of a flat gold surface. Figure 2(b) is taken from a grating

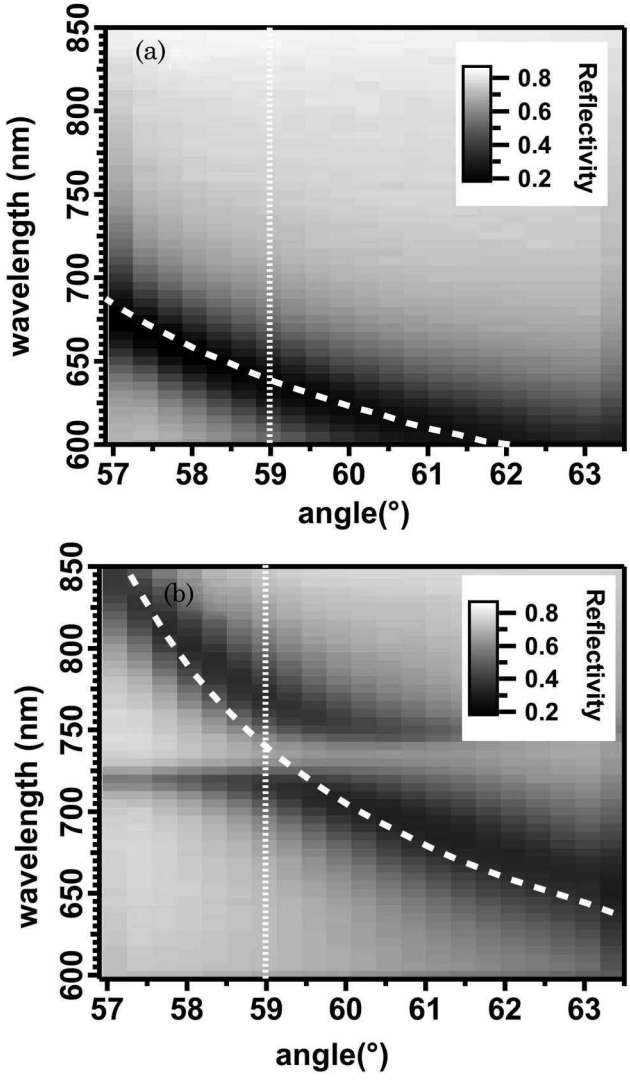

Fig. 2. Normalized spectro-angular SPR reflectivity maps of the sample surface (a) in the uniform gold region and (b) in a grating region. Dashed curves: SPR spectral profiles shown in Fig. 3, at 59° incidence. Dotted lines: surface plasmon wave theoretical dispersion relation for (a) uniform gold and (b) for an equivalent dielectric layer corresponding to the grating.

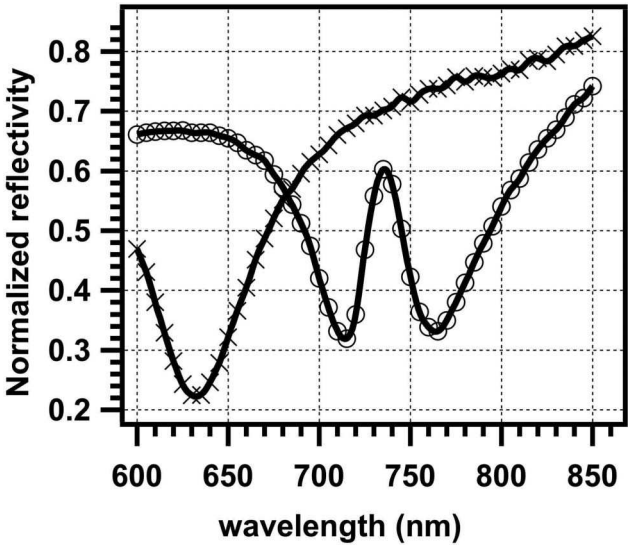

Fig. 3. SPR spectral profile plots at 59° incidence: crosses, in the uniform gold region; circles, in the grating region. Symbols represent data points; curves are interpolations of the data.

area, and a surface plasmon bandgap centered on 735 nm is clearly visible. SPR spectral profiles taken at 59° incidence are depicted in Fig. 3 and are represented as dotted lines on the maps of Fig. 2.

Near the surface plasmon bandgap of Fig. 2(b), the reflectivity is almost independent of the angle of incidence. This behavior can be used for bandgap-assisted sensing [7], where compact setups can be designed. At fixed angles near the surface plasmon bandgap, tuning the wavelength will excite different resonant modes of the gratings. In Fig. 3, the resonance dips at 715 and 776 nm correspond to a coupling of the surface plasmon modes between the gold and the low (water) and high (PMMA ridges) refractive index media [11].

An angulo-spectral SPRI system has been developed. It is based on a classical Kretschmann–Raether configuration with a spectrally tunable light source. Complete spectro-angular reflectivity maps can be obtained from the acquired SPR images. PMMA one-dimensional grating regions were fabricated on a gold surface using electron beam lithography and characterized using our multiparametric SPRI setup. The reflectivity maps obtained show a surface plasmon bandgap in the grating regions.

We thank Philippe Lalanne for the program based on RCWA used to simulate the reflectivity of line gratings. This work is partially supported by the European network of Excellence Photonics4Life, part of the FP7 framework.

References

1. J. Homola, Chem. Rev. **108**, 462 (2008).
2. A. Duval, A. Laisné, D. Pompon, S. Held, A. Bellemain, J. Moreau, and M. Canva, Opt. Lett. **34**, 3634 (2009).
3. F. Bardin, A. Bellemain, G. Roger, and M. Canva, Biosens. Bioelectron. **24**, 2100 (2009).
4. C. J. Alleyne, A. G. Kirk, W. Y. Chien, and P. G. Charette, Opt. Express **16**, 19493 (2008).
5. M. Nakkach, P. Lecaruyer, F. Bardin, J. Sakly, Z. B. Lakhdar, and M. Canva, Appl. Opt. **47**, 6177 (2008).
6. M. G. Manera, J. Spadavecchia, A. Taurino, and R. Rella, J. Opt. **12**, 035003 (2010).
7. P. Lisboa, A. Valsesia, I. Mannelli, S. Mornet, P. Colpo, and F. Rossi, Adv. Mater. **20**, 2352 (2008).
8. A. J. Benahmed and C. M. Ho, Appl. Opt. **46**, 3369 (2007).
9. X. D. Hoa, A. G. Kirk, and M. Tabrizian, Biosens. Bioelectron. **24**, 3043 (2009).
10. S. J. Yoon and D. Kim, J. Opt. Soc. Am. A **25**, 725 (2008).
11. W. L. Bares, T. W. Presis, S. C. Kitson, J. R. Sambles, N. P. K. Cotter, and D. J. Nash, Phys. Rev. B **51**, 11164 (1995).